OTC-26922-MS

Smart Novel Semi-Active Tuned Mass Damper for Fixed-Bottom and Floating Offshore Wind

A. Rodriguez Tsouroukdissian, GE Renewable Energy; S. Park, P. Pourazarm, W. La Cava and M. Lackner, University of Massachusetts; S. Lee and J. Cross-Whiter, Glosten Associates.

Abstract

The intention of this paper is to present the results of a novel smart semi-active tuned mass damper (SA-TMD), which mitigates unwanted loads for both fixed-bottom and floating offshore wind systems. The paper will focus on the most challenging water depths for both fixed-bottom and floating systems. A close to 38m Monopile and 55m Tension Leg Platform (TLP) will be considered. A technical development and trade-off analysis will be presented comparing the new system with existing passive non-linear TMD (N-TMD) technology and semi-active. The SA-TMD works passively and activates itself with low power source under unwanted dynamic loading in less than 60msec. It is composed of both variable stiffness and damping elements coupled to a central pendulum mass. The analysis has been done numerically in both FAST (NREL) and Orcaflex (Orcina), and integrated in the Wind Turbine system employing CAD/CAE. The results of this work will pave the way for experimental testing to complete the technology qualification process. The load reductions under extreme and fatigue cases reach up significant levels at tower base, consequently reducing LCOE for fixed-bottom to floating wind solutions. The nacelle acceleration is reduced substantially under severe random wind and sea states, reducing the risks of failure of electromechanical components and blades at the rotor nacelle assembly. The SA-TMD system is a new technology that has not been applied previously in wind solutions. Structural damping devices aim to increase offshore wind turbine system robustness and reliability, which eases multiple substructures installations and global stability. The paper is part of the US Department of Energy grant # DE-EE0005494.

Introduction and Background

The global offshore wind industry is poised to set a record for annual installations in 2015 (Aaron Smith, 2015). Although only 1,069 megawatts (MW) of new capacity was installed in 2014, 2015 is expected to be a record year for offshore wind deployments globally, with 3,996 MW on track to begin operations. In the first half of 2015, the industry commissioned 1,190 MW of this capacity, bringing the total current installed capacity to 8,990 MW worldwide. The global cumulative capacity is expected to reach 11,800 MW by year-end 2015. A review of project announcements suggests that cumulative global offshore wind capacity could grow to more than 47,000 MW by 2020. Although the majority of this capacity is being built in Europe, the industry is becoming more geographically dispersed with projects now under construction in the Asian and U.S. markets, like Block Island Wind Farm by Deepwater Wind.

Most of the current offshore projects are installed in water depths up to 40m and up to 120km from shore as seen in (Aaron Smith, 2015). However, the current pipeline will grow to deeper water depths and farther from shore, which produces several technological challenges, especially in the substructure and wind turbine performance. The portfolio of fixed-bottom to floating substructures typology can be condensed into six main types as seen in Figure 1. From the six main typologies, as mentioned in (Aaron Smith, 2015), it can be seen that 75% of the fully commissioned 8.9GW have Monopiles as the selected substructure and up to 66% in the announced projects.

Moreover, 7% of the 16GW announced projects have chosen a floating substructure as the technology for those selected sites, which could grow even more as part of the 22.39GW potential seen in Figure 1.

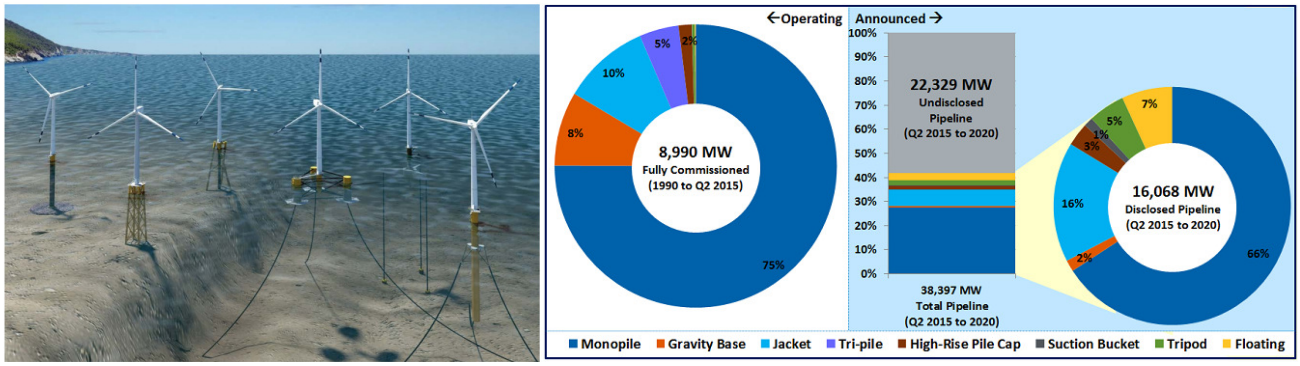

Figure 1 - Offshore wind substructure designs for varying water depths. Illustration by Josh Bauer, NREL and Global offshore wind substructure market share (Aaron Smith, 2015)

Compared to its fixed-bottom counterparts, the Monopile has a simple and relatively cost-effective design. On the other hand, due to its large diameter, Monopile wave-structure interaction becomes more acute compared to a wave transparent Jacket, for example. Monopiles are highly dominated by the geometry variation of the system due to water depth, external excitations (wind & wave), and boundary conditions, and consequently been very sensitive to global natural frequencies changes. In particular, its undamped 1st bending side-to-side mode, as seen in Figure 2, is easily excited by the wind and wave misaligned cases in power production or normal sea states, causing a significant increase of fatigue loads in both the tower and Monopile. These FLS challenges for deep water (close to 40m) Monopiles presents an opportunity to be solved by employing structural damping devices like a N-TMD, or a more advanced SA-TMD that may better control TMD excursions and add more damping to the system.

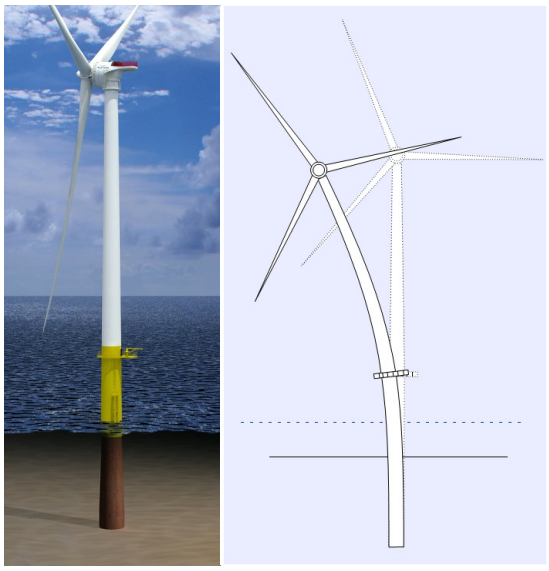

Figure 2 – GE Haliade150-6MW on a Monopile and 1st bending Side-to-Side mode in a Monopile fixed-bottom substructure (Mark L. Brodersen, 2014)

While the vision of large-scale floating wind turbines was introduced by (Heronemus, 1972), it was not until the mid-1990's, after the commercial wind industry was well established, that the topic was reconsidered by several research teams. Currently, fixed offshore substructures have reached deployment to water depths up to 40m, however, several floating substructures solutions may be more economical for water depths above 50m compared to their fixed-bottom counterparts. The concepts that have been studied up to now for offshore fixed and floating wind turbines resemble structures from the Oil & Gas industry. The floating substructure/platform

must provide the buoyancy to support the wind turbine and restrain within acceptable limits of the 6 DOF's -- surge, sway, heave, pitch, roll, and yaw. The floating wind turbine design philosophy may be impacted if platform dynamics require a more dynamically compliant system, but the platform cost is likely to dominate the cost trade-offs. The Tension Leg Platform (TLP) achieves its stability by a combination of both tendon tension and buoyancy, making it lighter compared to its other floating substructures counterparts (Spar Buoys, Semi-Submersible) as seen in Figure 3. However, at shallow waters (close to 55m) TLP's are highly sensitive to extreme wave impacts with a potential risk of having a slack line or losing tension in one of its tendons, which causes a large load increase in both the tower and central TLP column. These ULS challenges for shallow water TLP's present an opportunity to be solved by employing structural damping devices like a N-TMD or SA-TMD's for wider frequency dampening.

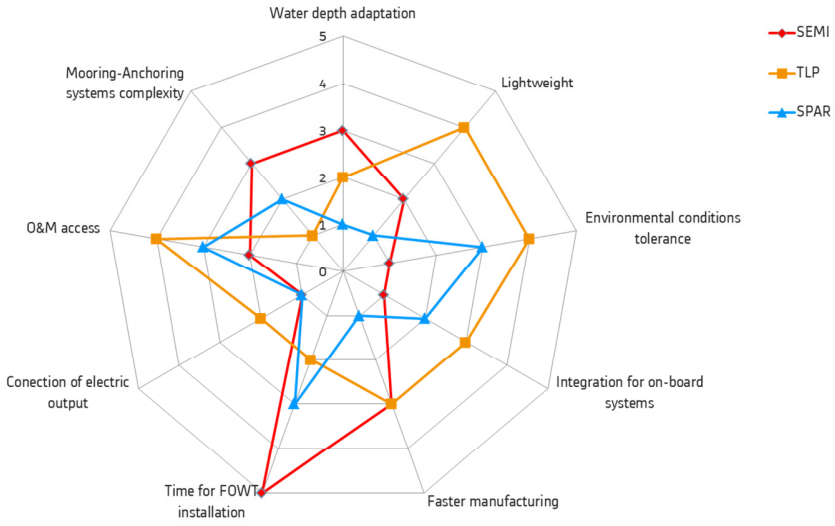

Figure 3 – GE Haliade 150-6MW on top of a Pelastar TLP by Glosten and a qualitative assessment of 3 floating substructures concepts

While much research has investigated the utilization of the conventional RNA (i.e. pitch, torque, etc.) control systems for load reduction in offshore wind turbines, structural damping control devices are a relatively new approach. Over the past 30 years, numerous structural control strategies and devices have been developed for civil engineering structures in order to mitigate loads caused by wind and earthquakes. In recent publications (Basu, 2014), structural control of wind turbines has been included among the many structural control applications. Recently, structural control has been investigated in offshore wind turbines, including floating turbines, using various kinds of tuned mass dampers (TMDs) such as translational tuned mass dampers, tuned liquid column dampers (TLCD) and pendulum tuned mass dampers (Lackner, 2011) and (Stewart, 2013). Innovative passive and semi-active structural damping control configurations like toggle brace damping augmentation systems, which differ from conventional TMDs, have been explored in (Tsouroukdissian, 2011), (Tsouroukdissian A. R., 2014) and (Brodersen, 2014).

In this study, the mathematical modeling for a pendulum-type TMD operating omni-directionally (fore-aft and side-to-side) developed by ESM GmbH was established and incorporated into the TMD module in FASTv8 (Jonkman, 2005) the wind turbine aero-elastic simulator developed by NREL. The performance of this damper located at the tower top of a wind turbine (GE Haliade 150-6MW) operating both passively, and semi-actively (with an on-off state damping ratio based on the ground hook control policy) are analyzed in the ultimate limit state (ULS) with parked rotor conditions and fatigue limit state (FLS) on both deep water Monopile and a shallow water TLP (Glosten Pelastar) using FASTv8. The impact of stroke limitations of the TMDs and the mooring line stiffness are evaluated as well.

Offshore Wind turbine System Description

Fixed-Bottom Offshore Wind Structure Numerical Model

In this study the Monopile support structure and GE Haliade 150-6MW wind turbine were chosen to model the fixed-bottom offshore wind turbine structure. The tower diameter is 4m at the top and 6m at the base. The Monopile has a diameter of 6m at platform height (approx. +16.00m), which increases gradually up to 8m at the mudline (approx. -37.00m). The portion of the Monopile embedded into the soil has a constant diameter of 8m and extends for 32m. The turbine structural parameters are listed in Table 1.

Table 1 - Physical parameters of GE Haliade 6-MW Wind Turbine

Rated Power	6MW
Cut-in wind speed	3 m/s
Cut-out wind speed	25 m/s
Rotor Orientation	Upwind
Rotor Diameter	150 m
Hub Height	100 m
Rotor Speed Range	4 - 11.5 rpm
Generator Type	Direct Drive Permanent Magnet
Gear Box	None
Power Control System	Variable speed, independent pitch control

The wind turbine and Monopile are modeled using the time-marching aero-elastic code FASTv8 developed by NREL. The wind turbine structure is defined using the ElastoDyn module, which considers the first two fore-aft and side-to-side modes of the tower and the first two flapwise and the first edgewise modes of the blades to calculate the structural loadings and displacements. The support structure is modeled using the SubDyn module through defining joints, elements and their properties, as well as the number of modes to be retained. FASTv8 used the AeroDyn module, based on blade-element momentum (BEM) theory, to calculate the aerodynamics of the rotor. The hydrodynamic loads, from irregular waves and currents in offshore wind turbines, are calculated using the HydroDyn module, through using a combined potential flow and Morison's equation formulation. The Monopile soil-structure interaction is modeled by employing the apparent fixity method to obtain the same tower natural frequency and displacement at mud-line. The soil characteristics of this site are mix of sand and clay. The tower's first and second fore-aft and side-to-side natural frequencies are 0.246 Hz and 0.77 Hz respectively.

Floating Offshore Wind Structure Numerical Model

The floating platform modeled in this study is Glosten's PelaStar tension leg platform (TLP), coupled with the GE Haliade 150-6MW turbine. This floating wind turbine system was designed for the Wave Hub test site off the coast of Cornwall, UK, in a FEED study sponsored by the Energy Technology Institute of Loughborough, UK. The platform was designed in accordance with DNV specifications (DNV, 2014). A simulation model of the platform was developed in OrcaFlex and used to derive FLS and ULS loads in the ETI study. In this model the tower, central column and arms of the platform were modeled by elastic line elements, with hydrodynamic forces defined by Morison's equation. The central hull was defined by multiple rigidly-coupled buoys, with hydrodynamic forces defined by Morison's equation. The aerodynamic thrust of the turbine was modeled by a drag force applied at the turbine hub position. This model was validated in operating and idling conditions against 1/50 scale physical model tests (Vita et al 2015).

To improve the modeling of the aerodynamics and rotating machinery in operating conditions a simulation model for the FAST v8 software was developed by NREL. This model was based on the Glosten Orcaflex model, but it included detailed representations of the turbine blades, rotor aerodynamics and nacelle mechanical components. This FAST model formed the basis of the FLS model used in the simulations reported herein. The NREL FAST model also formed the basis for the FAST ULS model, used by University of Massachusetts for developing TMD

models. The FLS model assumed the mean water level at the Wave Hub site (58.5m), and the ULS model was developed for the extreme low water condition (54.7m). That depth was found in the ETI project to lead to the most severe structural loads on the column and tower. The ULS simulations were all in 50-year return period conditions, so the turbine was idling. The platform particulars are summarized in Table 2.

Table 2 - Particulars of PelaStar with GE Haliade 150-6MW

Arm radius	31.5 m
Low water design draft	21.0 m
Mean design draft	25.6 m
High water design draft	30.1 m
Installed mass of platform	1729 T
High water displacement	5001 m3
Low water displacement	4639 m3
Tower interface height	52.6 m above baseline

Passive & Semi-Active Structural Control Modeling

Structural Damper Characteristics

In this study, the impacts of a pendulum-type N-TMD and SA-TMD, located at the tower-top, are investigated using the TMD module of FASTv8. The TMD designed by ESM GmbH, has a moving mass of 20,000 kg, mass ratio of 3.3%, tuned to the 1st bending frequency of the system and it oscillates omni-directionally. The natural frequency of the TMD is tuned to match the tower's first natural frequency in the fore-aft and side-to-side directions. The TMD oscillations absorb the energy of tower fore-aft and side-to-side motion, simultaneously. In the FASTv8 with TMD module, there are new features for deriving non-linear position constraints of a TMD (passive or SA), as well as semi-active control algorithms using ground-hook control policies. These non-linear position constraints of the TMDs can be achieved by applying a non-linear force-displacement curve defined in the TMD input file by the user, which can restrict TMD motion at some specific positions. For small displacements, the TMD oscillates at the tuning frequency in the linear stiffness region, and then a non-linear force curve is applied when the TMD excursion exceeds some defined limit, which is composed of a tri-linear stiffness representation developed by ESM GmbH composed of the regulation spring (first bi-linear region) and the stop springs (last stiffness slope).

Control Strategies of On-Off Semi-Active TMDs

The parameters (spring stiffness and damping constant) of N-TMDs are constant during operation, which may cause performance deterioration in some cases. The damping constant of the proposed SA-TMDs in this study can be controlled by two damping values - an ON and OFF state, which are determined by following specific control policies based on the relative velocity or displacement of the TMDs, and the absolute velocity of the primary structure. The formulations of the displacement-based ground-hook (DB-GH) control policy are as follows (Setareh, 2002) and (Koo, 2003).

$$x_{TTD}\dot{x}_{TMD} \leq 0 \quad Then \quad \zeta_{Controllable} = \zeta_{ON}\ (High\ Damping)$$

$$x_{TTD}\dot{x}_{TMD} > 0 \quad Then \quad \zeta_{Controllable} = \zeta_{OFF}\ (Low\ Damping)$$

, where, x_{TTD} is the tower top displacement, and $\dot{x}_{TMD}$ is the relative velocity between the TMD and the tower top. Another configuration of the ground-hook control algorithm, velocity-based ground-hook (VB-GH) depends on the absolute velocity of the tower top based on four conditions, summarized as follows:

- TMD in extension, pulling the tower to equilibrium (ζ_{ON})
- TMD in extension, pulling the tower from equilibrium (ζ_{OFF})
- TMD in compression, pushing the tower from equilibrium (ζ_{OFF})
- TMD in compression, pushing the tower to equilibrium (ζ_{ON})

The above four statements are expressed in the equations below:

$$\dot{x}_{TTD}\dot{x}_{TMD} \leq 0 \quad Then \quad \zeta_{Controllable} = \zeta_{ON}\ (High\ Damping)$$

$$\dot{x}_{TTD}\dot{x}_{TMD} > 0 \quad Then\ \zeta_{Controllable} = \zeta_{OFF}\ (Low\ Damping)$$

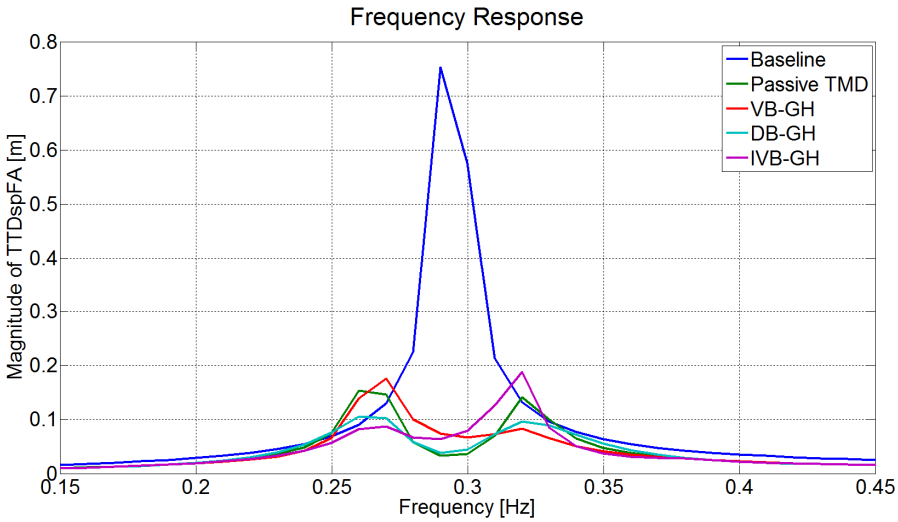

Figure 4 – Frequency response for tower top displacement

According to an initial perturbation analysis, the magnitude of the tower top displacement can be reduced using both DB-GH and VB-GH control policies compared to the passive type TMD as shown in Figure 4. The semi-active controller following the velocity based ground-hook control policy, however, has the largest response compared to the passive system in the lower frequency region region i.e. less than the resonant frequency (Viet, 2014). This phenomenon may cause a negative effect of the TMDs when the structure is excited by a wave spectrum, which is mostly distributed in the lower frequency region as shown in Figure 4. In the inverse velocity based ground-hook (IVB-GH) controller, the magnitude of the tower top displacement can be reduced significantly compared to other methods. This IVB-GH policy can be achieved with the opposite logic of the VB-GH controller shown in Figure 5, i.e. the switching between high and low damping states is the opposite of the VB-GH logic. Because of the predominantly low frequency loading on the structure due to the waves, the IVB-GH control algorithm is the method we focus on in this study. Figure 6 represents the basic block diagram of the ground-hook control algorithm, and how to apply the non-linear spring force according to the TMD positions. The controllable parameters are the TMD damping constant (On-Off state) and the TMD spring forces. The controllable damping constant can be calculated through the ground-hook control policy, using the tower and TMD motions. The non-linear spring forces can be calculated using the TMD displacement and the input force-displacement curve. These damping and spring forces act as reaction forces to the wind turbine tower.

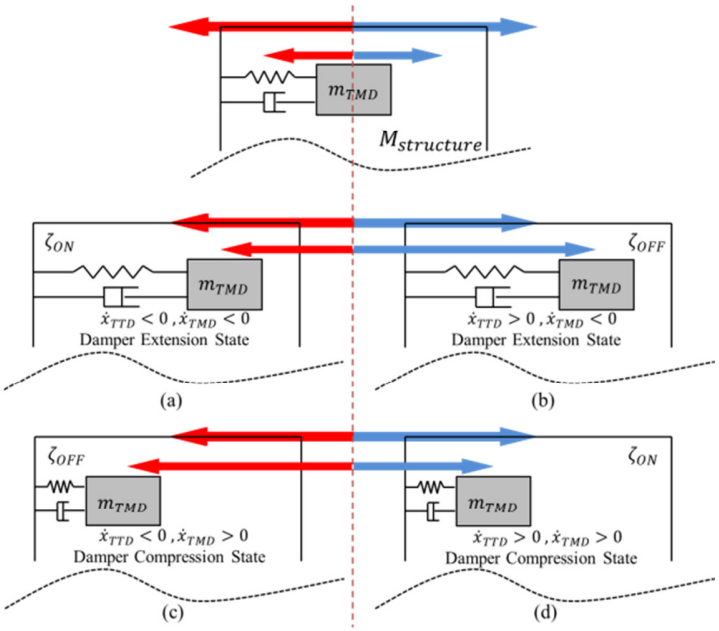

Figure 5 – Four conditions for inverse velocity based ground-hook control policy, (a) Extension TMD with $\dot{x}_{TTD} < 0$ (b) Extension TMD with $\dot{x}_{TTD} > 0$ (c) Compression TMD with $\dot{x}_{TTD} < 0$ (d) Compression TMD with $\dot{x}_{TTD} > 0$

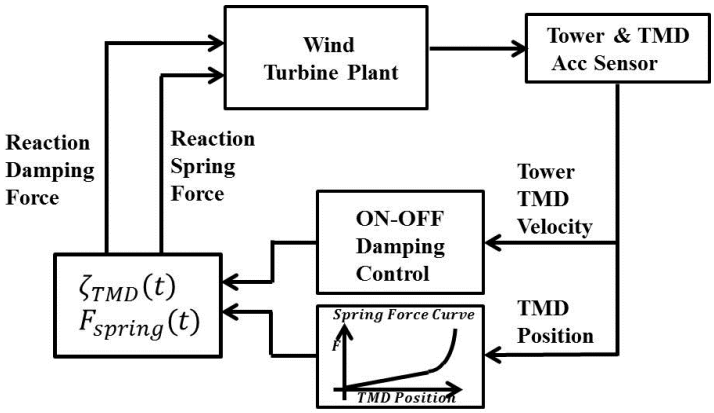

Figure 6 – Block diagram for semi-active ground-hook control algorithm and non-linear spring force calculation

The TMD was modeled in Orcaflex with a 20ton mass suspended on four horizontal support rods, parallel to the axes of the nacelle. These rods had very high bending stiffness in the vertical plane, to minimize the vertical deflections of the TMD, but essentially zero axial stiffness and zero bending stiffness in the horizontal plane, to minimize restraint on horizontal motions. The horizontal restraint forces provided by the regulation spring were modeled in two ways: horizontal springs with nonlinear stiffness and an external function with table look-ups of force versus deflection. In the N-TMD the dampers were modeled by horizontal linear dampers. In the SA-TMD the dampers were modeled by an external function providing the forces on the TMD and nacelle according to the IVB-GH equations discussed above. The TMD model in Orcaflex is shown in Figure 7.

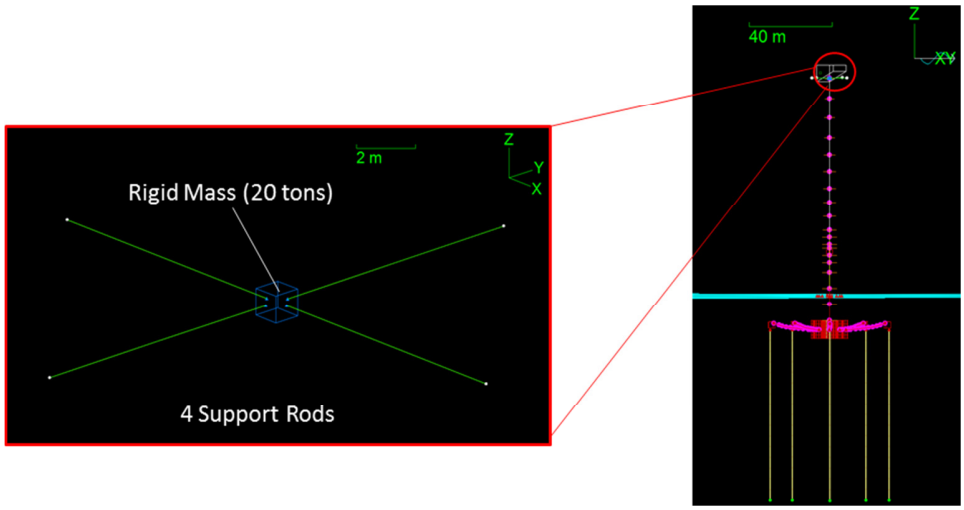

Figure 7 – TMD model in Orcaflex with a 20 ton mass suspended on four horizontal support rods

Monopile Integrated Loads & Structural Design

ULS and FLS design load cases were defined in order to thoroughly evaluate the performance of the N-TMD and the SA-TMD on ultimate and fatigue load reductions. The Monopile is located in the North Atlantic Ocean with water depth of approximately 37m. The driving ULS Design Load Case was identified as DLC 6.1a, which is a 50 year return period and mean wind speed of 41.5 m/s. The turbine is in an idling condition and the blades are pitched to 90 degrees. Three different wind/wave misalignments and two different water levels are defined for this DLC. For each combination of misalignment and water level, six simulations with different random seeds and assuming 0°, +8° and -8° yaw error were conducted. Table 3 summarizes the DLC 6.1a external conditions. DLC 1.2 is the driving DLC for FLS calculations following IEC Standard (61400-1, 2005-08). In this DLC, the turbine is in normal operating condition. The mean wind speed varies from 4m/s to 24 m/s. for each flow velocity four wind/wave misalignments is defined. For each combination of mean wind speed and wind/wave misalignment, six simulations with different random seeds and assuming 0°, +8° and -8° yaw error were performed. Table 3 summarizes the DLC 1.2 external conditions. All simulations are 650 seconds long.

Table 3 - DLC 6.1a and DLC 1.2 external conditions

DLC	Wind Speed	Turb. Int	Wind shear	wind / wave	Significant wave height	Peak spectral period	peak shape parameter	Current: wind generated Speed	Current: sub-surface speed	Water Level	Sim #
6.1a	41.50	11.00%	0.14	0°, 30°, 330°	4.700	9.200	2.386	0.354	1.200	4.15 / -4.5	36
1.2	4	25.40%	0.11	0°, 30°, 60°, 90°	0.37	3.79	1.00	--	--	0	264
	6	20.40%	0.11	0°, 30°, 60°, 90°	0.42	3.89	1.00	--	--		
	8	17.90%	0.11	0°, 30°, 60°, 90°	0.48	4.01	1.00	--	--		
	10	16.60%	0.11	0°, 30°, 60°, 90°	0.54	4.13	1.00	--	--		
	12	14.40%	0.11	0°, 30°, 60°, 90°	0.61	4.26	1.00	--	--		
	14	12.80%	0.11	0°, 30°, 60°, 90°	0.68	4.39	1.00	--	--		
	16	12.00%	0.11	0°, 30°, 60°, 90°	0.76	4.54	1.00	--	--		
	18	11.60%	0.11	0°, 30°, 60°, 90°	0.84	4.68	1.00	--	--		
	20	10.90%	0.11	0°, 30°, 60°, 90°	0.93	4.84	1.00	--	--		
	22	11.10%	0.11	0°, 30°, 60°, 90°	1.02	4.99	1.07	--	--		
	24	10.50%	0.11	0°, 30°, 60°, 90°	1.12	5.16	1.15	--	--		

Ultimate Limit State (ULS) System Response

Simulations with DLC 6.1a external conditions were performed for three cases of baseline (no TMD), N-TMD and SA-TMD. The ultimate load for each set of six seeds is defined as the absolute maximum load closest to the average of the absolute maximums between the six seeds. In order to study the TMD performance, forces and moments at the tower top, tower base, and mud-line are compared between the three cases. Tower top displacements and accelerations as well as TMD displacements are also discussed. Table 4 lists the ultimate forces and moments percentage load reductions obtained at the tower top for the passive and semi-active cases with respect to the Baseline loads. In the Fore-Aft (FA) direction (Fx and My), the N-TMD results in a 35% decrease in the ultimate force at the tower top while the SA-TMD results in an even larger decrease of 49%. In the Side-to-Side (StS) direction (Fy and Mx), the N-TMD acts more effectively in reducing the ultimate load compared to the SA-TMD (23% compare to 19% decrease). The ultimate loads in the FA direction are much larger than the StS direction. There is an increase in the force in the gravitational direction due to the added mass of the TMD (Fz). While moments in the StS direction are barely affected by the TMD implementation, in the FA direction both N-TMD and SA-TMDs result in a 5% decrease in the ultimate moment. The N-TMD reduces the ultimate torsional moment (Mz) more effectively than SA-TMD (8% compare to 5% decrease).

Table 4 - The ultimate loadings at the tower top location for N-TMD and SA-TMD compared to baseline

	Fx	Fy	Fz	Mx	My	Mz
Passive	-35%	-23%	4.1%	-0.22%	-5%	-8%
SA	-49%	-19%	4.2%	0.03%	-5%	-5%

As shown in Table 5, in the FA direction, the SA-TMD causes larger reductions in the ultimate loadings (51% decrease in Fx and 44% in my) compared to the N-TMD (37% decrease in Fx and 33% in My), while in the StS direction, both TMD control methods return very similar results (29% decrease in the Fy and 26% in the Mx). The reduction in the ultimate torsional moment is higher using the N-TMD (8%) compare to SA-TMD (4%).

Table 5 - The ultimate loadings at the tower base location for N-TMD and SA-TMD compared to baseline

	Fx	Fy	Fz	Mx	My	Mz
Passive	-37%	-31%	2%	-26%	-33%	-8%
SA	-51%	-29%	2%	-26%	-44%	-4%

As seen in Table 6, for both N-TMD and SA-TMDs result in the same amount of ultimate force reductions at the mud-line (15% decrease in Fx and about 4% in Fy). The SA-TMD causes a larger reduction in the ultimate moments at mudline (40% decrease in My and 17% in Mx) compared to the N-TMD (34% decrease in My and 15% in Mx). Similar to the tower top and tower base, the N-TMD is more effective in reducing the ultimate torsional moment (Mz) than the semi-active technology (10% decrease compared to 6%).

Table 6 - The ultimate loadings at the mud-line location for N-TMD and SA-TMD compared to baseline

	Fx	Fy	Fz	Mx	My	Mz
Passive	-15%	-6%	0.50%	-15%	-34%	-10%
SA	-15%	-4%	0.48%	-17%	-40%	-6%

Table 7 summarizes the ultimate yaw accelerations and tower top displacements the wind turbine undergoes for the N-TMD and SA-TMD. The semi-active control is more effective than the passive control in reducing the tower top acceleration (53% decrease compared to 41%) and displacement in the FA direction (39% decrease compared to 28%), while in the StS direction both technologies result in similar amount of reductions in acceleration (about 25% reduction) and displacement (about 20% reduction).

Table 7 - The ultimate yaw bearing acceleration and tower top displacement for baseline, N-TMD and SA-TMD

	Ax	Ay	TTDspFA	TTDspSS
Passive	-41%	-28%	-28%	-20%

	Ax	Ay	TTDspFA	TTDspSS
SA	-53%	-25%	-39%	-22%

Another important parameter is the TMD stroke. For strokes smaller than 0.65 m, the force-displacement relationship remains linear. For strokes between 0.65 m and 0.8 m, the mass enters the bi-linear regime and for strokes larger than 0.8 m, the mass hits the stop springs where the force-displacement relationship is highly nonlinear. It is desirable to minimize the amount of time the TMD undergoes strokes larger than 0.8 m. Figure 8 shows TMD displacement for a sample ULS simulation. The dashed line shows the boundaries of the bi-linear region and solid line shows the boundaries of the nonlinear region. Considering all the simulations, for 14.15% of the time the passive TMD undergoes strokes larger than 0.65 m, while for 3.13% of the time the strokes are larger than 0.8 m. In the SA-TMD, the mass spends less time in the bi-linear and nonlinear regions compare to the N-TMD; it has strokes larger than 0.65m 7.43% of the time and strokes larger than 0.8m 1.36% of the time.

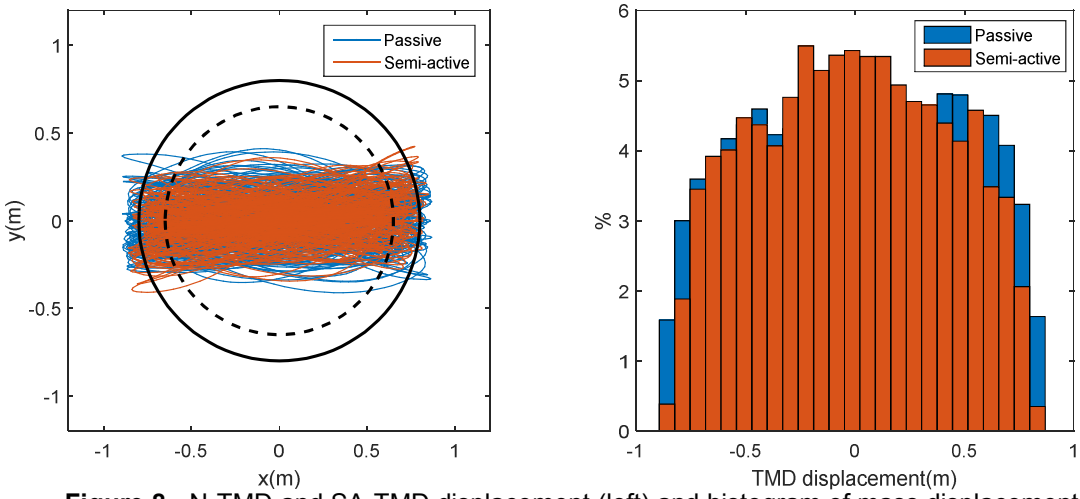

Figure 8 - N-TMD and SA-TMD displacement (left) and histogram of mass displacement (right)

Fatigue Limit State (FLS) System Response

Simulations with DLC 1.2 external conditions were performed for three cases of Baseline, N-TMD and SA-TMD. To evaluate the performance of each case, life-time damage equivalent loads were calculated at the tower top and tower base assuming S/N curve slopes of 3, 4, 5, 6, 7, 8, 9, and 10. The lifetime probability of each simulation was estimated based on the Weibull probability for the mean wind velocity and the corresponding probability of wind/wave misalignment shown in Figure 9. The structure is designed to have a lifetime of 25 years. The lifetime damage equivalent loads are defined as the load range of an equivalent sinusoidal load that results in the same amount of damage at 10^7 cycles.

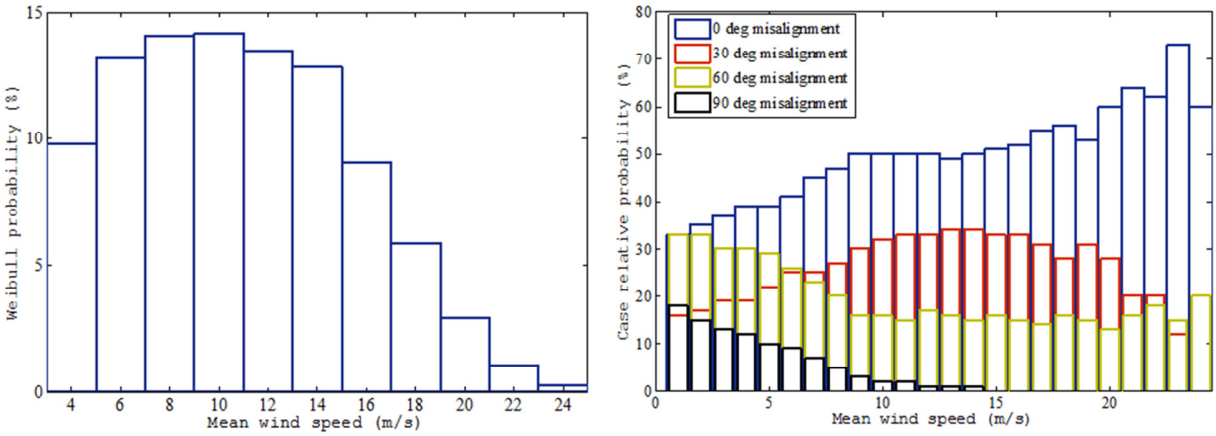

Figure 9 - Wind speed distribution (left) and wind/wave misalignment probability at each wind speed (right)

Table 8 and Table 9 show the amount of reduction in DELs obtained after implementation of N-TMD and SA-TMD, respectively. Specifically, at the tower base for m=3, significant reductions of -69% for Mx and -39% for My are achieved employing an N-TMD. The SA-TMD showed also the same amount of reduction for m=3 at tower base (-67% for Mx and -37% for My). Other components of the wind turbine will benefit from reductions in these loads as well. Figure 10 shows the damage representation at the tower base in a polar plot and the improvement of damage reduction by employing passive and semi-active dampers, which reduced damage values below 1. The plot shows welded damage values and no need for weld improvement using structural damping devices was considered. Also, the SA-TMD is activated during the FLS cases around 32% of the time in the Fore-Aft direction and 31% in the Side-to-Side direction, which will dimension the power source of the system.

Table 8 - The FLS loadings at the Monopile tower base location for passive TMD

S/N curve slope	Fx	Fy	Fz	Mx	My	Mz
m=3	-38%	-67%	1%	-69%	-39%	-22%
m=4	-41%	-68%	1%	-69%	-42%	-24%
m=5	-43%	-68%	1%	-68%	-43%	-25%
m=6	-45%	-67%	0%	-66%	-44%	-25%
m=7	-46%	-65%	0%	-65%	-45%	-25%
m=8	-47%	-64%	0%	-64%	-46%	-24%
m=9	-48%	-63%	0%	-63%	-47%	-24%
m=10	-48%	-63%	0%	-62%	-47%	-23%

Table 9 - The FLS loadings at the Monopile tower base location for semi-active TMD

S/N curve slope	Fx	Fy	Fz	Mx	My	Mz
m=3	-36%	-65%	1%	-67%	-37%	-21%
m=4	-39%	-67%	1%	-68%	-40%	-23%
m=5	-42%	-68%	1%	-69%	-42%	-24%
m=6	-43%	-69%	1%	-70%	-43%	-24%
m=7	-45%	-70%	1%	-70%	-44%	-24%
m=8	-46%	-70%	1%	-70%	-45%	-24%
m=9	-47%	-70%	1%	-71%	-46%	-23%
m=10	-47%	-71%	1%	-71%	-46%	-23%

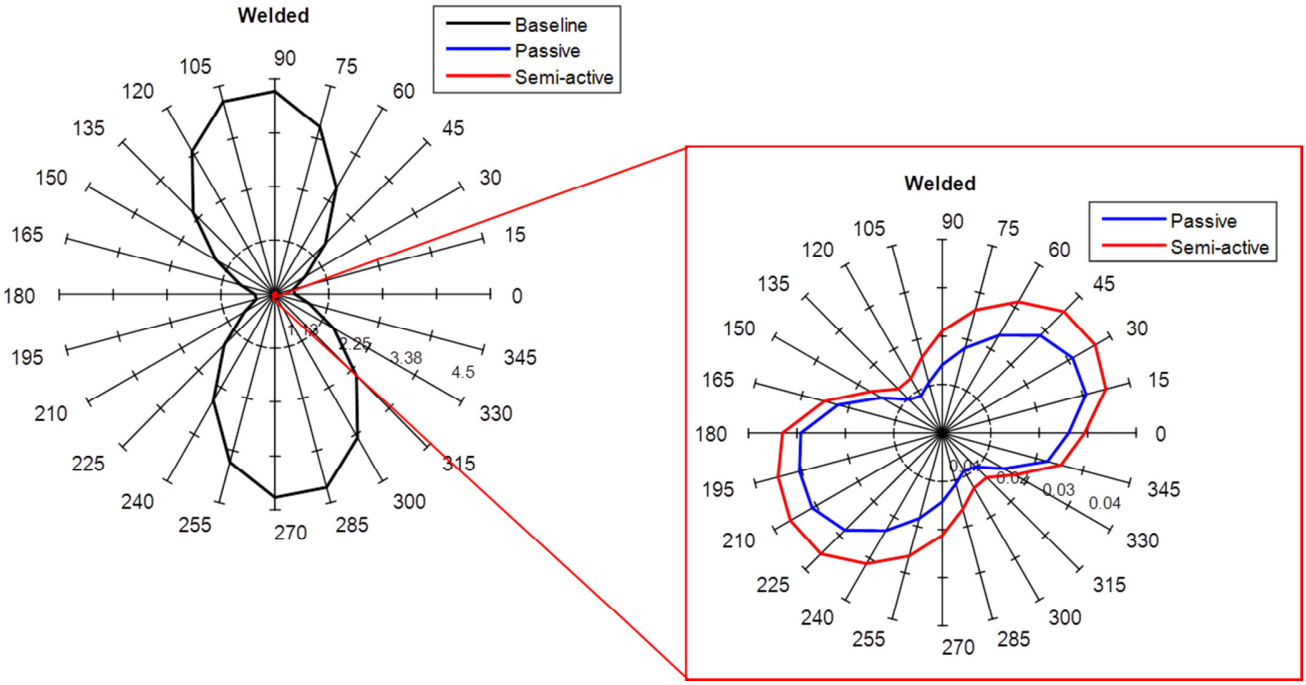

Figure 10 - Tower base damage (left) and passive and semi-active TMD response (right)

TLP Integrated Loads & Structural Design

The Wave Hub site, permitted as a test site for wave energy devices, has relatively severe wave conditions and shallow water for TLP technology, with a mean water level of 58.5m and extreme low water level of 54.7m. The environmental conditions for the TLP analysis were based on those developed for the ETI project. Wind, wave and current statistics were derived from site measurements and hind cast data by HR Wallingford hydraulics laboratory in the UK. ULS and FLS wind conditions were taken from statistical analyses of 30 year and 10 year hind cast wind data sets. Wave conditions were taken from wave hind casts and computations, using wave propagation models calibrated by measured wave data near the site. A FORM analysis of the wave data yielded a 50-yer return period contour of Hs and Tp, which was modified by Glosten to provide conservative estimates of 50-year return period structural responses on the PelaStar platform. The modified contour is shown in Figure 11.

It was found that the wave conditions near the highest significant wave height, 9.93 m and 10.26m, provided the governing structural loads, so these conditions were used in the ULS simulations in this analysis. The 50-year return period 10-minute average wind speed is 39.5 m/s at the hub. This wind speed is above the cut-out speed for the turbine, so the turbine was idling in all ULS cases. Wind and waves were collinear in all ULS conditions. For some responses the worst-case wind/wave heading is with one arm directed upwind, and for other responses the worst heading is with one arm directed downwind. These orientations are 36 deg apart in the 5-arm TLP (with a 72 deg angle between arms), so ULS cases at wind/wave headings of 0 and 36 deg were analyzed, to ensure worst-case conditions were studied.

To derive FLS conditions the wind and wave data were binned into a sequence of 6 wind speeds, 3 wave heights and 4 wave model period bins, giving a total of 42 environmental conditions, of which 35 are within the turbine operating wind speed range. The waves at the Wave Hub site are highly directional so all waves were conservatively assumed to come from the same direction for fatigue loads. Wind-wave misalignment was represented by two misalignment directions: 0 deg and 90 deg.

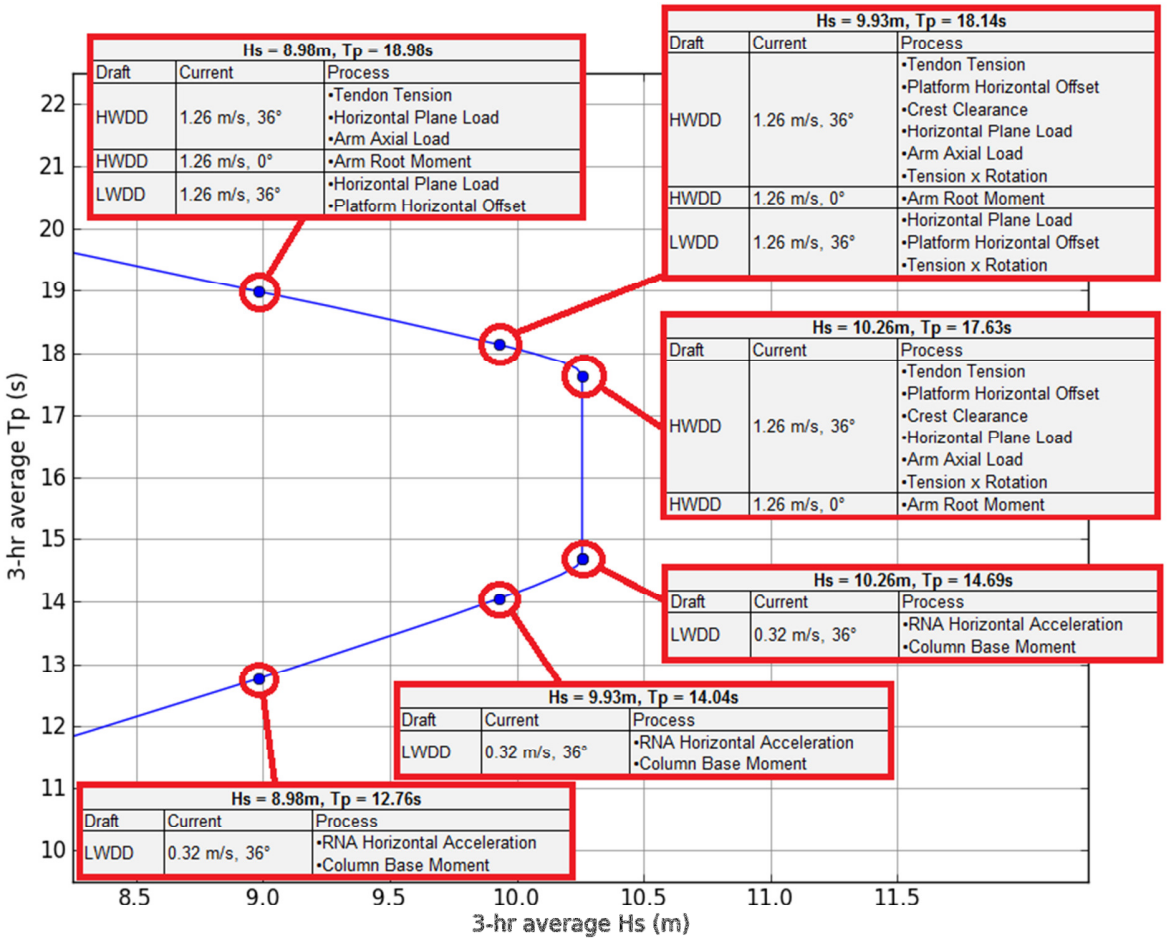

Figure 11 - 50-year return period wave height and period contour

Ultimate Limit State (ULS) System Response

The structural damping devices, both passive and semi-active, show an increase of the tower base load as seen in Table 10, which is contrary to what has been seen in the Monopile in previous sections. However, the shallow water TLP under such wave excitation is within a non-linear regime. Orcaflex simulations have been performed in order to show the differences between FAST and Orcaflex, and how these non-linearties are captured. Indeed as seen in Figure 12, Orcaflex does show a reduction in tower base loads when employing both damper technologies. This comparison was also tested for 100m water depth and better agreement between FAST and Orcaflex was obtained.

Table 10 – FAST ULS at the tower base location for passive and semi-active TMD compared to baseline

	Fx	Fy	Fz	Mx	My	Mz
Passive	2%	2%	2%	3%	3%	3%
SA	2%	2%	2%	3%	2%	3%

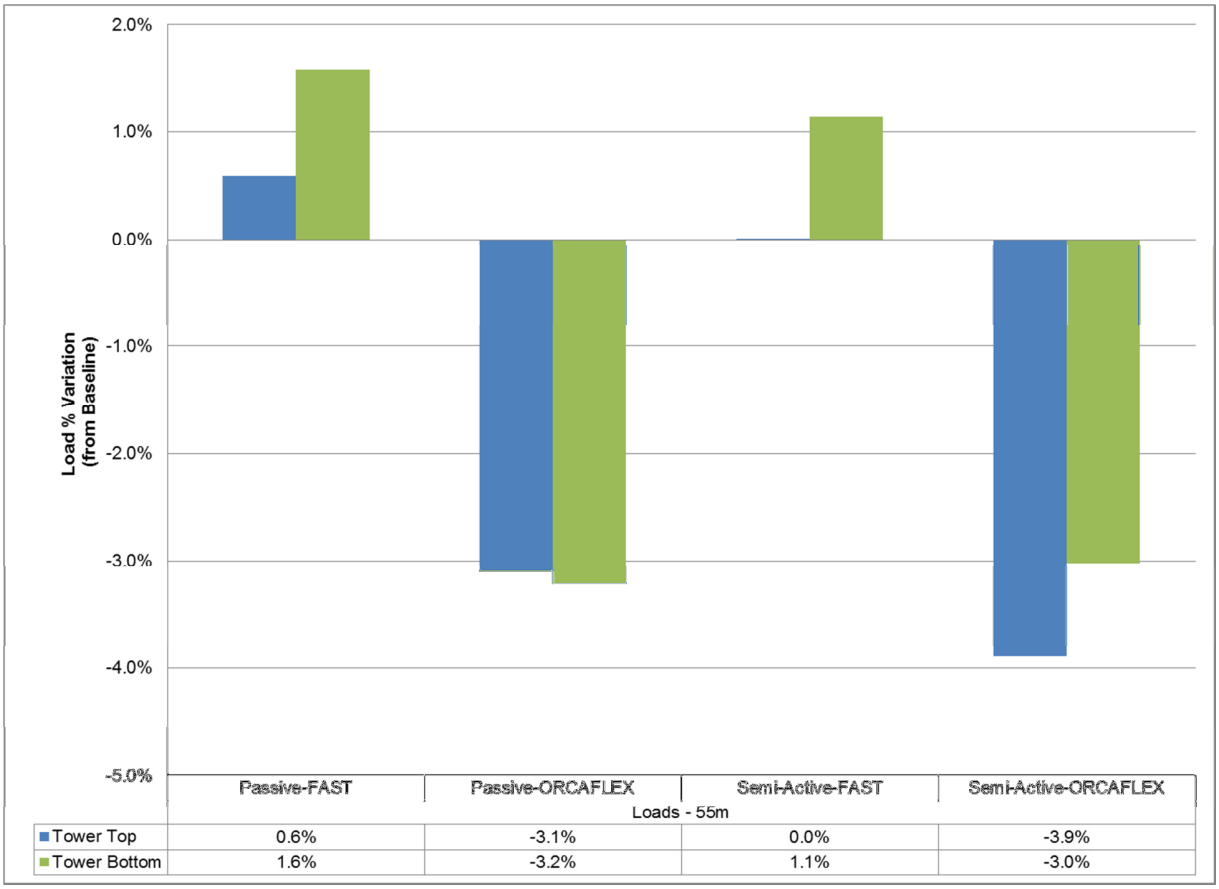

Figure 12 – ULS FAST vs Orcaflex tower base load comparison for both passive and semi-active TMD

As shown in Figure 12, Orcaflex shows 3.2% and 3.0% reductions of the tower base moments for both the N-TMD and SA-TMD, respectively, compared to increased loads from FAST of 1.6% and 1.1%. Table 11 demonstrates the variation of the acceleration due to the structural damper technologies. Similarly to the previous FAST and Orcaflex load comparison, Figure 13 shows a discrepancy between the two codes for tower top accelerations; for the Passive TMD the loads differ from -0.5% to -5.5% and for the SA-TMD from -1.9% to -6.8%. Again this did not happen for a 100m case and this may be due to the dynamic response of the system.

Table 11 – FAST ULS tower top displacement for baseline, passive TMD and semi-active TMD

	Ax	Ay	TTDspFA	TTDspSS
Passive	2%	0%	3%	3%
SA	-0.3%	-1%	2%	3%

A crucial parameter for a TLP design, especially at shallow water, is to avoid a slack line event under ULS conditions. Both the N-TMD and SA-TMD avoided slack line events, which otherwise occurred for the baseline system.

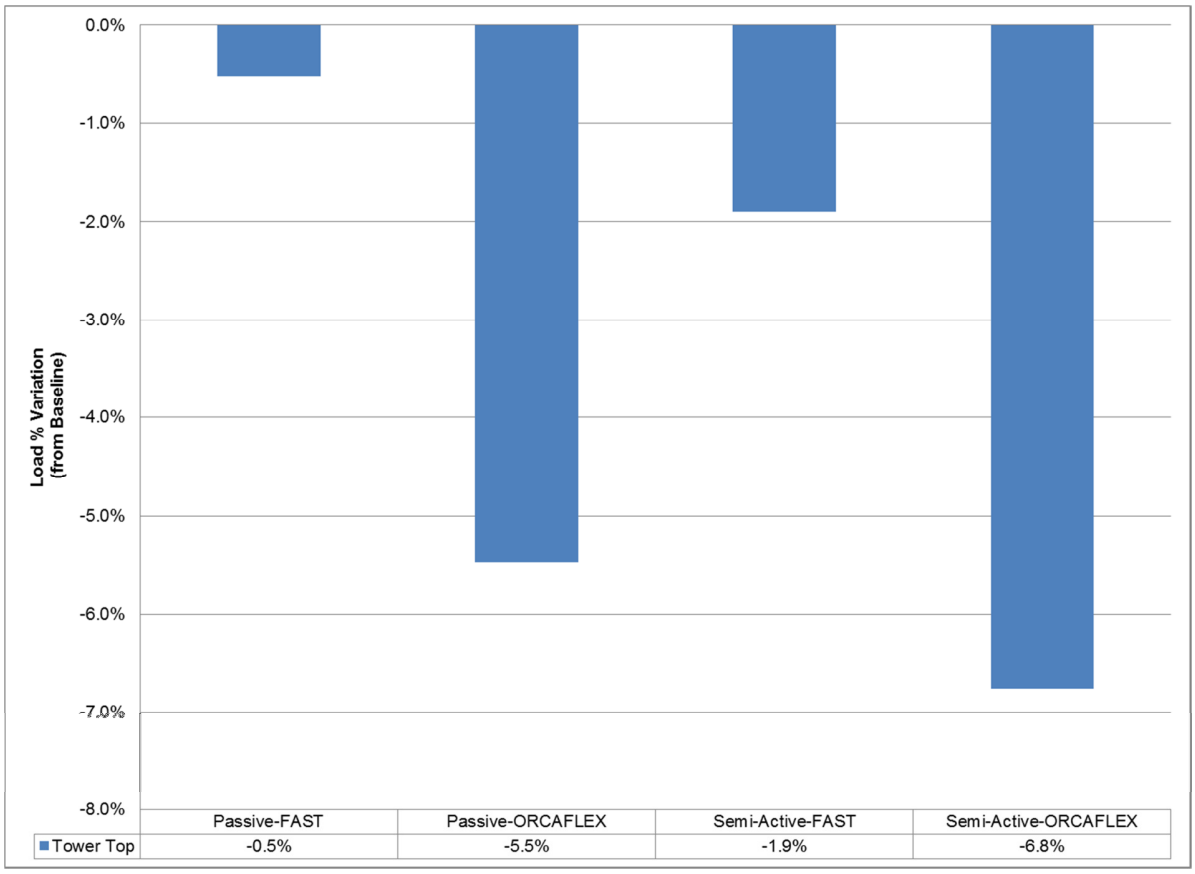

Figure 13 - ULS FAST vs Orcaflex tower top RNA Acceleration comparison for both passive and semi-active TMD

Fatigue Limit State (FLS) System Response

Table 12 and Table 13 show the amount of reduction in DELs obtained after implementation of the N-TMD and SA-TMD, respectively. Specifically, at the tower base with m=3, a significant reduction of -41% for Mx and -10% for My occurs when employing a N-TMD. The SA-TMD shows similar reduction for m=3 at the tower base of -41% for Mx and -11% for My. Figure 14 shows the damage representation at the tower base in a polar plot and damage reduction by employing passive and semi-active dampers, which reduce damage values down to 0.04 in Side-to-Side (Mx) compared to the baseline maximum values of 0.32. On the other hand, for the shallow water TLP case the Fore-Aft (My) direction is slightly reduced from 0.85 to 0.6, which still is below 1 and should not undergo weld improvement like grinding and/or hammer penning to reduce damage. The SA-TMD is activated during the FLS cases around -63% of the time in the Fore-Aft direction and -51% in the Side-to-Side direction, which will dimension the power source of the system.

Table 12 - The FLS loadings at the TLP tower base location for passive TMD

S/N curve slope	Fx	Fy	Fz	Mx	My	Mz
m=3	-5%	-28%	-1%	-41%	-10%	-19%
m=4	-3%	-26%	-1%	-41%	-6%	-19%
m=5	-1%	-23%	-0.1%	-41%	-3%	-19%
m=6	0.1%	-21%	0.1%	-41%	-1%	-18%
m=7	1%	-19%	0.2%	-41%	0.3%	-18%
m=8	1%	-18%	0.3%	-41%	1%	-17%
m=9	1%	-17%	0.3%	-40%	2%	-17%
m=10	1%	-16%	0.4%	-40%	2%	-17%

Table 13 - The FLS loadings at the TLP tower base location for semi-active TMD

S/N curve slope	Fx	Fy	Fz	Mx	My	Mz
m=3	-5%	-28%	-1%	-41%	-11%	-19%
m=4	-3%	-25%	-1%	-40%	-7%	-19%
m=5	-1%	-23%	-0.1%	-40%	-4%	-19%
m=6	0.2%	-21%	0.1%	-40%	-1%	-18%
m=7	1%	-19%	0.1%	-40%	0.3%	-18%
m=8	1%	-18%	0.2%	-41%	1%	-17%
m=9	1%	-17%	0.2%	-41%	2%	-17%
m=10	1%	-17%	0.3%	-40%	2%	-17%

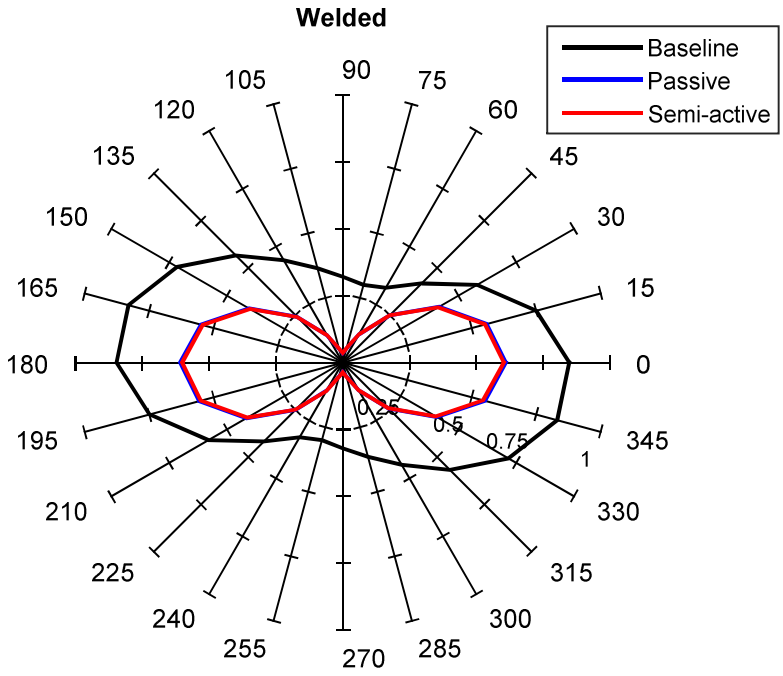

Figure 14 - Tower base damage for baseline, passive and semi-active TMD response

Conclusions

The performance of both a deep water fixed-bottom Monopile and shallow water TLP have been analyzed successfully while employing a passive TMD and semi-active TMD dampers. The use of structural damping devices reduced the ULS loads in the Monopile more effectively than in the shallow water TLP, due to nature of the dynamic response and also the environmental conditions to which both systems were exposed. For FLS loads the structural damping devices performed more effectively in the Monopile than in TLP, while being activated less time compared to TLP's. Moreover, as the water depth increases for a TLP, the effectiveness of the structural damping devices increases significantly. On the other hand, the structural damping devices in both the Monopile and TLP contribute to a robust and reliable design, by reducing large damage values in Side-to-Side in the Monopile, and avoiding slack line events in the TLP.

This work gives rise to further exploration of advanced structural control damper configurations (Tsouroukdissian, 2011), (Tsouroukdissian A. R., 2014) and (Brodersen, 2014), different control schemes, numerical code improvement, and advanced materials performance. Moreover, due to the high uncertainty and multi-criteria decision analysis (Kolios, Tsouroukdissian, & K., 2014), this work opens the door for a future reliability and risk based design framework (Muskulus, 2015), to analyze optimally (Muskulus M. &., 2014) the effect of dampers with respect to soil-structure interaction, different substructure types, different water depth, wind and wave loads.

Acknowledgements
This material is based upon work supported by the Department of Energy under Award Number # DE-EE0005494. Thanks to the co-authors for their excellent work, Dhiraj Arora as GE DOE Principal Investigator, Ty Murray as GE DOE Project Manager, Albert Fisas as GE Project Sponsor, and Jonathan Mechineau as GE TMD Product Project Manager and his team. Special thanks to Karl Hanus from ESM GmbH for the TMD detailed design, Rick Damiani and Bonnie Jonkman from NREL for their fruitful feedback on FAST model.

Disclaimer

References
1. 61400-1, I. (2005-08). *Wind turbines – Design Requirements 3rd Edition.* IEC.
2. Basu, B., Bursi, O., Casciati, F., Casciati, S., Del Grosso, A., Domaneschi, M., et al. (2014). A European Association for the Control of Structures joint perspective. Recent studies in civil structural control across Europe. *Structural Control and Health Monitoring 21(12)*.
3. Brodersen, M., & J., H. (2014). Damping of offshore wind turbine tower vibrations. *EERA DeepWind'2014, 11th Deep Sea Offshore Wind R&D Conference, Energy Procedia 53*, (pp. 258–267). Trondheim, Norway.
4. DNV. (2013). *DNV-OS-J103 - Design of Floating Wind Turbines .* DNV.
5. DNV. (2014). *DNV-OS-J101 - Design of Offshore Wind Turbines Structures.* DNV.
6. Heronemus, W. E. (1972). Power from Offshore Winds. *Proceedings of the 8th Annual Conference of the Marine Technology Society.* Washington, DC.
7. Jonkman, J., & L., B. J. (2005). *FAST user's guide.* Golden, CO: National Renewable Energy Laboratory Technical Report No. NREL/EL-500-38230.
8. Kolios, A., Tsouroukdissian, A., & Salonitis, K. (2014). Multi-criteria decision analysis of offshore wind turbines support structures under stochastic inputs. *Ships and Offshore Structures*, 2-12.
9. Koo, J. H. (2003). *Using magneto-rheological dampers in semiactive tuned vibration absorbers to control structural vibrations.* Ph.D. thesis, Virginia Polytechnic Institute and State University.
10. Lackner, M., & M.A., R. (2011). Passive structural control of offshore wind turbines. *Wind energy 14(3)*, 373-388.
11. Muskulus, M. S. (2014). Design optimization of wind turbine support structures - A review. *Journal of Ocean and Wind Energy*, 12-22.
12. Muskulus, M. S. (2015). Reliability-based design of wind turbine support structures. *Symposium on Reliability of Engineering System, SRES'2015*, (pp. 1-13). Hangzhou, China.
13. Setareh, M. (2002). Floor vibration control using semi-active tuned mass dampers. *Canadian Journal of Civil Engineering, 29(1)*, 76-84.
14. Smith, A., Stehly, T., & Musial, W. (2015). *2014-2015 Offshore Wind Technologies Market Report.* NREL.
15. Stewart, G., & Lackner, M. (2013). Offshore wind turbine load reduction employing optimal passive tuned mass damping systems. *IEEE Transactions on Control Systems Technology, 21(4)*, 1090-1104.
16. Tsouroukdissian, A. R. (2014). *Patent No. 8,641,369 B2.* US.
17. Tsouroukdissian, A. R., Carcangiu, C., Pineda, I. F., Kuhnle, B., Scheu, M., & M., M. (2011). Wind Turbine Structural Damping Control for Tower Load Reduction. *IMAC XXIX A Conference and Exposition on Structural Dynamics.* Jacksonville, FL: ASME.
18. Viet, L., Nghi, N., Hieu, N., Hung, D., Linh, N., & L.X., H. (2014). On a combination of ground-hook controllers for semi-active tuned mass dampers. *Journal of Mechanical Science and Technology, 28(6)*, 2059-2064.
19. Vita, L., Ramachandran, G., Krieger, A., Kvittem, M., Merino, D., Cross-Whiter, J., et al. (2015). Comparison of Numerical Models and Verification Against Experimental Data, Using PelaStar TLP Concept. *Proceedings of the ASME 2015 34th International Conference on Ocean, Offshore and Arctic Engineering.* OMAE2015-41874.